

## Nanoparticles

## Supramolecular Fluorescent Nanoparticles Constructed via Multiple Non-Covalent Interactions for the Detection of Hydrogen Peroxide in Cancer Cells

Xuan Wei,<sup>[a]</sup> Ruijiao Dong,<sup>[a]</sup> Dali Wang,<sup>[a]</sup> Tianyu Zhao,<sup>[b]</sup> Yongsheng Gao,<sup>[b]</sup> Patrick Duffy,<sup>[b]</sup> Xinyuan Zhu,<sup>\*[a]</sup> and Wenxin Wang<sup>\*[b]</sup>

**Abstract:** Overabundance of hydrogen peroxide originating from environmental stress and/or genetic mutation can lead to pathological conditions. Thus, the highly sensitive detection of H<sub>2</sub>O<sub>2</sub> is important. Herein, supramolecular fluorescent nanoparticles self-assembled from fluorescein isothiocyanate modified  $\beta$ -cyclodextrin (FITC- $\beta$ -CD)/rhodamine B modified ferrocene (Fc-RB) amphiphile were prepared through host-guest interaction between FITC- $\beta$ -CD host and Fc-RB guest for H<sub>2</sub>O<sub>2</sub> detection in cancer cells. The self-assembled nanoparticles based on a combination of multiple non-covalent interactions in aqueous medium showed high sensitivity to H<sub>2</sub>O<sub>2</sub> while maintaining stability under physiological condi-

tion. Owing to the fluorescence resonance energy transfer (FRET) effect, addition of H<sub>2</sub>O<sub>2</sub> led to obvious fluorescence change of nanoparticles from red (RB) to green (FITC) in fluorescent experiments. In vitro study showed the fluorescent nanoparticles could be efficiently internalized by cancer cells and then disrupted by endogenous H<sub>2</sub>O<sub>2</sub>, accompanying with FRET from "on" to "off". These supramolecular fluorescent nanoparticles constructed via multiple non-covalent interactions are expected to have potential applications in diagnosis and imaging of diseases caused by oxidative stresses.

## Introduction

Hydrogen peroxide (H<sub>2</sub>O<sub>2</sub>) is a kind of reactive oxygen species (ROS) endogenously generated in living organisms, which is increasingly recognized as a small-molecule mediator of various physiological processes.<sup>[1]</sup> However, during times of environmental stress, ROS levels can increase dramatically, which may lead to significant damage to cell structures and pathological conditions including cancers,<sup>[2]</sup> diabetes,<sup>[3]</sup> cardiovascular diseases,<sup>[4]</sup> and neurodegenerative disorders like Alzheimer's, Parkinson's, and Huntington's diseases.<sup>[5]</sup> In particular, H<sub>2</sub>O<sub>2</sub> levels in cancer cells are elevated up to  $1-5 \times 10^{-5}$  M compared with  $0.5-7 \times 10^{-7}$  M in normal cells.<sup>[6]</sup> The difference between oxidiz-

ing extracellular environment and reducing cytosol in cancer cells provides an opportunity to detect intracellular H<sub>2</sub>O<sub>2</sub>.

For the past few years, a variety of designing strategies have been developed for H<sub>2</sub>O<sub>2</sub> detection based on chemiluminescence,<sup>[7]</sup> fluorescence,<sup>[8]</sup> and electrochemical<sup>[9]</sup> techniques. Among all these designing strategies, covalently bonded materials are robust but uncontrollable when exposed to external stimuli, susceptible to damage and difficult to reversibly reform, while non-covalent bonds can enable facile construction of stimuli-responsive supramolecular materials with capacity to undergo reversible changes for various biomedical applications.<sup>[10]</sup> However, the weak non-covalent interactions and the operational instability of supramolecular systems have shown to be the main disadvantages.<sup>[10a]</sup> Therefore, we deduce that if the robustness of supramolecular H<sub>2</sub>O<sub>2</sub> sensors is improved, a promising stable and sensitive supramolecular system for intracellular H<sub>2</sub>O<sub>2</sub> detection can be expected. Therefore we propose that self-assembly of a supramolecular amphiphile<sup>[11]</sup> in aqueous medium based on a combination of multiple non-covalent interactions (hydrophilic/hydrophobic and host-guest interactions) can improve robustness, controllability, and adaptability of H<sub>2</sub>O<sub>2</sub> detection systems.

Herein, we describe the design and construction of a supramolecular nanoparticle reactive toward cellular H<sub>2</sub>O<sub>2</sub> by the complexation of  $\beta$ -CD and Fc as a key step (Scheme 1). First, RB-modified Fc derivative (Fc-RB) forms stable one to one complexes in aqueous solution with FITC-modified  $\beta$ -CD (FITC- $\beta$ -CD) by penetrating of Fc guest into the internal hydrophobic

[a] X. Wei, R. Dong, D. Wang, Prof. X. Zhu  
School of Chemistry and Chemical Engineering  
State Key Laboratory of Metal Matrix Composites  
Shanghai Jiao Tong University  
800 Dongchuan Road, Shanghai 200240 (P.R. China)  
Fax: (+86) 21-54741297  
E-mail: xyzhu@sjtu.edu.cn

[b] T. Zhao, Y. Gao, P. Duffy, Dr. W. Wang  
Charles Institute of Dermatology  
School of Medicine and Medical Science  
University College Dublin  
Belfield, Dublin 4 (Ireland)  
Fax: (+353) 1-7166341  
E-mail: wenxin.wang@ucd.ie

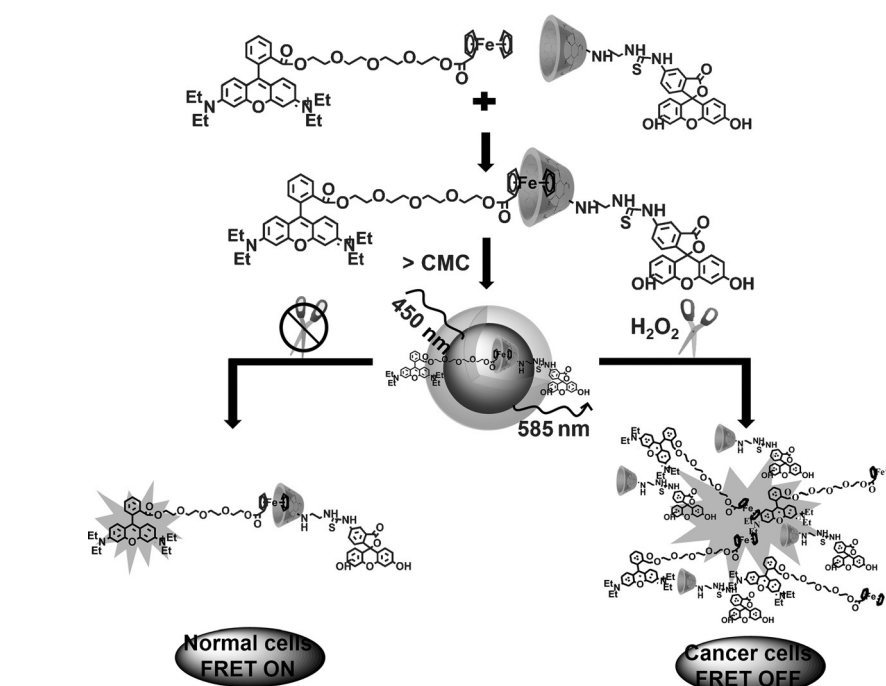
Supporting information for this article is available on the WWW under <http://dx.doi.org/10.1002/chem.201501317>.

cavity of the  $\beta$ -CD host, so that FRET<sup>[12]</sup> is “on” (red fluorescence). The inherent amphiphilicity of the FITC- $\beta$ -CD/Fc-RB makes it possible to self-assemble into stable nanoparticles under physiological conditions, benefiting from the collaborative stabilization of hydrophobic interaction. Then the FITC- $\beta$ -CD/Fc-RB nanoparticles can be internalized by cancer cells and disrupted by endogenous levels of  $H_2O_2$ , FITC- $\beta$ -CD/Fc-RB nanoparticles can detect  $H_2O_2$  in cancer cells by the change of fluorescence from red to green, owing to FRET effect from “on” to “off”.

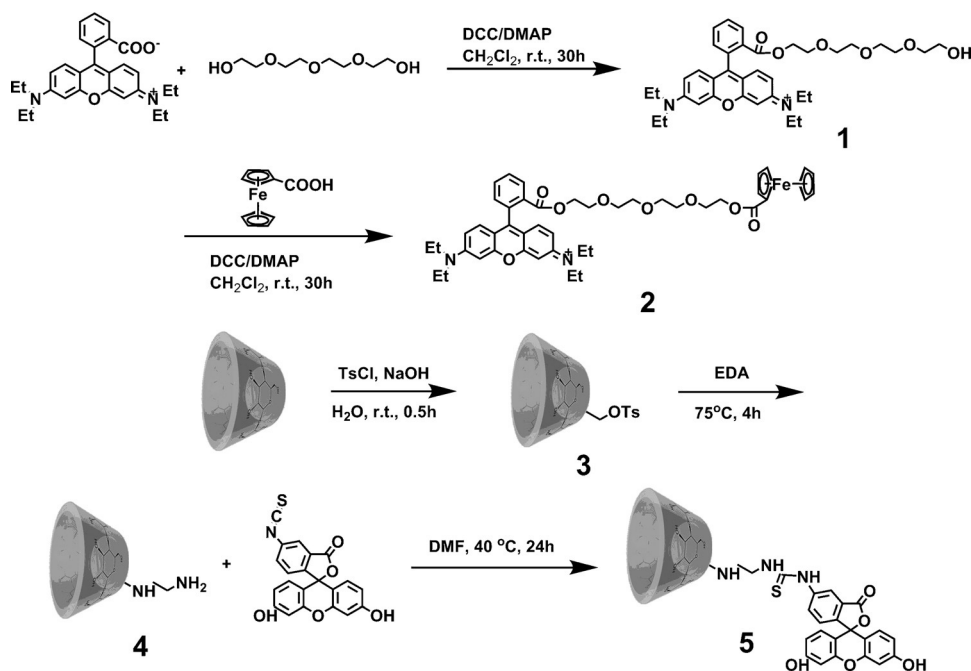
## Results and Discussion

### Synthesis and characterization

The synthetic routes used to obtain Fc-RB guest (2) and FITC- $\beta$ -CD host (5) are illustrated in Scheme 2. For the guest segment, compound 1 was first synthesized by the reaction of tetraglycol with RB in the presence of dicyclohexylcarbodiimide (DCC) and 4-dimethylaminopyridine (DMAP) in  $CH_2Cl_2$ , followed by a reaction with equimolar amounts of ferrocenecarboxylic acid in  $CH_2Cl_2$  to obtain the desired compound 2. For the host segment, compound 4 was prepared according to the literature procedure<sup>[13]</sup> and then reacted with FITC in dimethylformamide (DMF). The successful preparation of Fc-RB guest and FITC- $\beta$ -CD host was confirmed by <sup>1</sup>H NMR, <sup>13</sup>C NMR, UV/Vis and Q-TOF-MS. The carbon atom signals at  $\delta = 171.01$  and 165.19 ppm in the <sup>13</sup>C NMR spectrum of Fc-RB guest (2) (Figure S2) are assigned to the Ph-C=O and Cp-C=O of Fc-RB guest (2), respectively. Figure S3 shows a strong absorption band at 1710  $cm^{-1}$  in accordance with the carbonyl group in the FTIR spectrum, which further confirms the successful preparation of Fc-RB guest (2). The peak at  $\delta = 180.95$  ppm in the <sup>13</sup>C NMR spectrum (Figure S6) is attributed to the carbon atom of NH-C=S of FITC- $\beta$ -CD host (5). The detailed characterization data are described in Figures S1–S8 in the Supporting Information.



Scheme 1. FITC- $\beta$ -CD/Fc-RB amphiphile and its  $H_2O_2$ -activated behavior.



Scheme 2. Synthetic routes of RB-modified Fc (Fc-RB, 2) and FITC-modified  $\beta$ -CD (FITC- $\beta$ -CD, 5).

### Host-guest interaction

It has been widely reported that  $\beta$ -CD hosts can complex with Fc guests based on the host-guest interaction.<sup>[14]</sup> Therefore, it can be inferred that FITC- $\beta$ -CD host and Fc-RB guest might form supramolecular amphiphile with FRET effect. Here, 2D ROESY <sup>1</sup>H NMR was used to study the host-guest interaction of FITC- $\beta$ -CD and Fc-RB. According to the 2D ROESY <sup>1</sup>H NMR

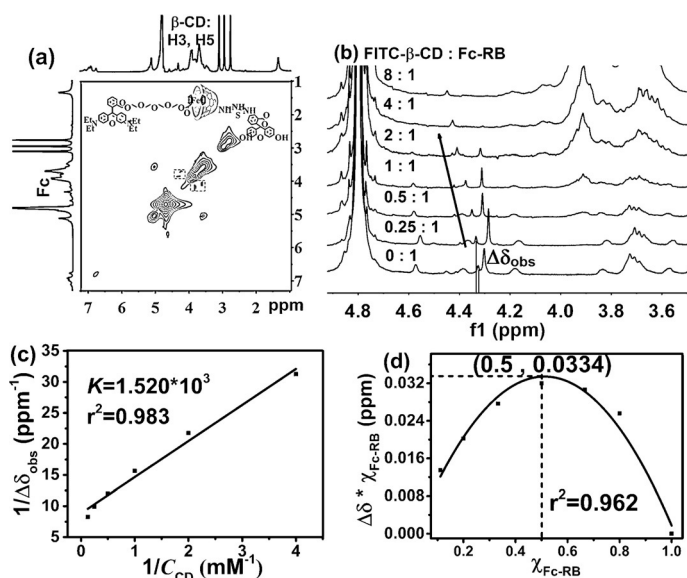


**Figure 1.** a) 2D ROESY  $^1\text{H}$  NMR spectrum of an equimolar mixture of the FITC- $\beta$ -CD and Fc-RB in  $[\text{D}_6]\text{DMSO}/\text{D}_2\text{O}$  (2/3, v/v) at 10 mm at  $30^\circ\text{C}$ ; b)  $^1\text{H}$  NMR spectra of FITC- $\beta$ -CD and Fc-RB at different molar ratios of 0:1, 0.25:1, 0.5:1, 1:1, 2:1, 4:1 and 8:1 in  $[\text{D}_6]\text{DMSO}/\text{D}_2\text{O}$  (2:3, v/v). The concentration of Fc-RB is  $1\text{ mM}$ ; c)  $^1\text{H}$  NMR spectrum of  $1/\Delta\delta_{\text{obs}}$  against  $1/C_{\text{CD}}$ ; d) Job's plot of FITC- $\beta$ -CD and Fc-RB.  $\chi_{\text{Fc-RB}}$  is the molar fraction of Fc-RB in the FITC- $\beta$ -CD/Fc-RB mixture.

spectrum of an equimolar mixture of FITC- $\beta$ -CD and Fc-RB in  $[\text{D}_6]\text{DMSO}/\text{D}_2\text{O}$  (2:3, v/v) at 10 mm in Figure 1a, the Fc proton signals (4.2 ppm) are correlated with signals of the inner protons of  $\beta$ -CD (3.8 ppm), proving the formation of the inclusion complexation between FITC- $\beta$ -CD and Fc-RB.

The host-guest interaction of FITC- $\beta$ -CD and Fc-RB was further confirmed by  $^1\text{H}$  NMR analysis.<sup>[15]</sup> In Figure 1b, the chemical shift of the Fc proton of Fc-RB increases accordingly with the increase of molar ratio of FITC- $\beta$ -CD:Fc-RB from 0:1 to 8:1, further indicating the complexation of FITC- $\beta$ -CD with Fc-RB. With the help of the  $^1\text{H}$  NMR spectra, the reciprocals of the peak shifts for Fc proton signals of Fc-RB ( $1/\Delta\delta_{\text{obs}}$ ) were determined and then plotted against the reciprocals of the FITC- $\beta$ -CD concentrations ( $1/C_{\text{CD}}$ ). According to the Figure 1c, there's a good linear correlation between FITC- $\beta$ -CD and Fc-RB, implying that the host-guest interaction of FITC- $\beta$ -CD with Fc-RB is on the foundation of the 1:1 inclusion complexes. According to the calculated slope and the intercept of the linear line, the association constant  $K$  for the one to one complexes of the FITC- $\beta$ -CD host with the Fc-RB guest in  $[\text{D}_6]\text{DMSO}/\text{D}_2\text{O}$  (2:3, v/v) is determined to be  $1.5 \times 10^3\text{ M}^{-1}$  by:

$$\frac{1}{\Delta\delta_{\text{obs}}} = \frac{1}{K\Delta\delta_{\text{CD}}} + \frac{1}{\Delta\delta}$$

where  $\Delta\delta$  is the discrepancy between the observed chemical shift for the 1:1 complexes of FITC- $\beta$ -CD with Fc-RB and the chemical shift without FITC- $\beta$ -CD. Moreover, the binding stoichiometry of FITC- $\beta$ -CD to Fc-RB was also calculated by  $^1\text{H}$  NMR. According to the Job's plot of  $\Delta\delta \times \chi_{\text{Fc-RB}}$  vs.  $\chi_{\text{Fc-RB}}$  in Figure 1d, the peak is about 0.5, implying that the binding sto-

ichiometry of FITC- $\beta$ -CD host to Fc-RB guest is 1:1. Thus, the results above successfully verify the formation of the one to one FITC- $\beta$ -CD/Fc-RB inclusion complexes.

### Formation and stability of self-assembled nanoparticles

After confirming the host-guest interaction of FITC- $\beta$ -CD host and Fc-RB guest, the self-assembly behavior of the supramolecular FITC- $\beta$ -CD/Fc-RB amphiphile was further investigated. The inherent amphiphilicity of the FITC- $\beta$ -CD/Fc-RB makes it possible to self-assemble into nanoparticles in aqueous solution. In order to investigate the self-assembly behavior of FITC- $\beta$ -CD/Fc-RB in aqueous solution, the critical micelle concentration (CMC) was measured. The relationship of the fluorescence intensity with the FITC- $\beta$ -CD/Fc-RB concentration is presented in Figure 2a. The excitation wavelength and the emission wavelength were set at 450 nm and 580 nm respectively. At low FITC- $\beta$ -CD/Fc-RB concentration, the fluorescence intensity remains nearly unchanged; with the enhancement of FITC- $\beta$ -CD/Fc-RB concentration, the fluorescence intensity starts to increase dramatically at a certain FITC- $\beta$ -CD/Fc-RB concentration. Based on the inflexion of the curve, the CMC of FITC- $\beta$ -CD/Fc-RB is about  $11.44\ \mu\text{g mL}^{-1}$  ( $4.75\ \mu\text{M}$ ), indicating the aggregation of supramolecular FITC- $\beta$ -CD/Fc-RB amphiphiles.

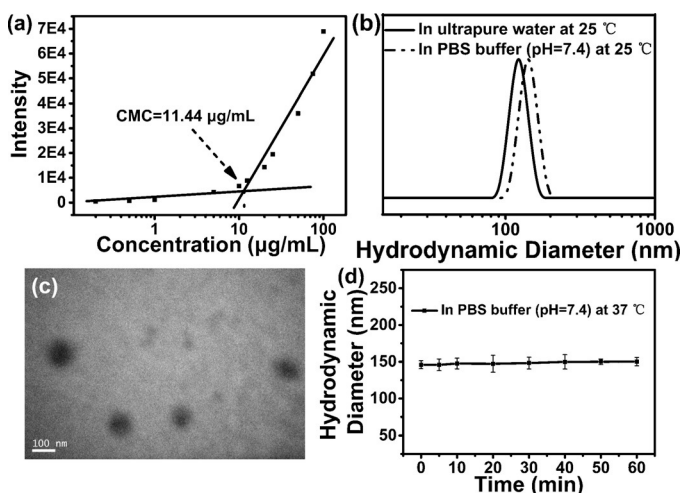


**Figure 2.** a) CMC measurement of FITC- $\beta$ -CD/Fc-RB; b) size variation of nanoparticles in different solvents at  $25^\circ\text{C}$  by DLS; c) TEM image of nanoparticles; d) time-dependent size variation of nanoparticles in PBS buffer (pH 7.4) at  $37^\circ\text{C}$ . Black bars represent the mean values ( $n=3$ ).

In order to investigate the morphology and size of the self-assembled FITC- $\beta$ -CD/Fc-RB aggregates, a DMF solution of the FITC- $\beta$ -CD/Fc-RB amphiphile was added slowly into aqueous solution and then dialyzed against water to remove DMF. After 24 h, the solution was diluted by adding ultrapure water to 20 mL to obtain an aggregate solution with a final concentration of  $200\ \mu\text{M}$ . Figure 2b shows the dynamic light scattering curve of FITC- $\beta$ -CD/Fc-RB aqueous solution, indicating the formation of nanoparticles with an average hydrodynamic diameter of approximately 122 nm. Transmission electron microscopy

(TEM) was further used to investigate the morphology of the nanoparticles. According to the TEM image in Figure 2c, the average size of the spherical nanoparticles is about 110 nm. The difference between the sizes measured by DLS and TEM is owing to the shrinkage of the nanoparticles in drying state during the TEM sample preparation. The stability of the nanoparticles was then detected by the real-time DLS. As can be seen in Figure 2d, the size of FITC- $\beta$ -CD/Fc-RB nanoparticles (148 nm) increases slightly in phosphate-buffered saline (PBS, pH 7.4, physiological conditions) at 37 °C due to the strong ion effect. Also Figure 2d shows that the size of nanoparticles is almost unchanged in PBS solution (pH 7.4) at 37 °C for 1 h, suggesting that the high stability of self-assembled nanoparticles in physiological conditions is due to the collaborative stabilization of hydrophobic interaction.

### Optical and sensing properties

The DLS and TEM data verify that the FITC- $\beta$ -CD/Fc-RB amphiphile could self-assemble into nanoparticles in water, which are very stable under physiological conditions. Subsequently, the fluorescence-based sensing properties of the nanoparticles to H<sub>2</sub>O<sub>2</sub> were detected. The UV/Vis measurement in Figure 3 shows that the maximum absorptions of FITC- $\beta$ -CD and Fc-RB are located at 494 and 560 nm, respectively. For the self-assembled FITC- $\beta$ -CD/Fc-RB nanoparticles, both UV/Vis absorption peaks can be observed. The UV/Vis spectrum is referential for choosing appropriate fluorescence excitation wavelength in the following experiments, in which the excitation wavelength was set at 450 nm.

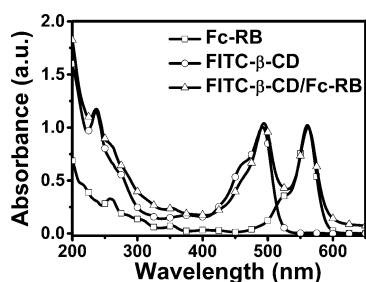


**Figure 3.** UV/Vis spectra of FITC- $\beta$ -CD, Fc-RB, and FITC- $\beta$ -CD/Fc-RB in ultrapure water.

The fluorescent performance of FITC- $\beta$ -CD/Fc-RB nanoparticles in water was investigated and the excitation wavelength was set at 450 nm.<sup>[8c]</sup> Figure 4a gives the fluorescence emissions of FITC- $\beta$ -CD, Fc-RB, and FITC- $\beta$ -CD/Fc-RB nanoparticles. Here, FITC (donor) and RB (acceptor) were conjugated with  $\beta$ -CD host and Fc guest, respectively. After the self-assembly of FITC- $\beta$ -CD/Fc-RB amphiphile, the supramolecular nanoparticles display strong FRET effect, which can be visualized through the

strong emission from the acceptor (RB, ~585 nm) and low emission from the donor (FITC, ~515 nm). In the presence of H<sub>2</sub>O<sub>2</sub>, cleavage of FITC- $\beta$ -CD/Fc-RB amphiphile and subsequent collapse of supramolecular nanoparticles can destroy the FRET effect, accompanying with the decrease in the acceptor emission (~3-fold) and increase in donor emission (~7-fold), as shown in Figure 4b. The combined ~20-fold change could

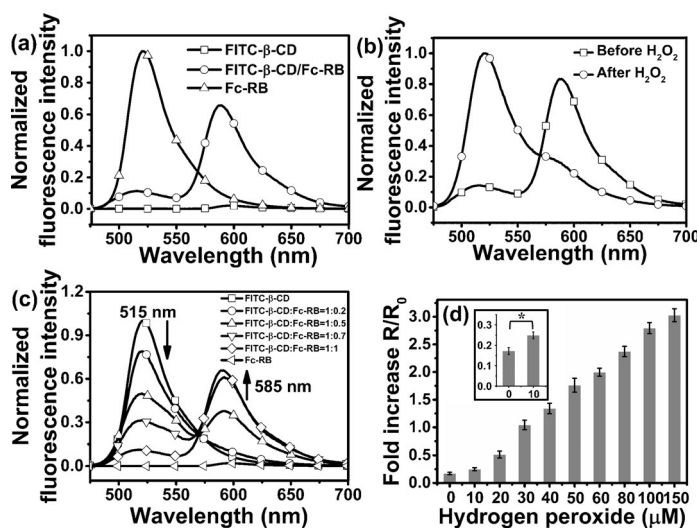


**Figure 4.** a) Fluorescence emissions of FITC- $\beta$ -CD (1  $\mu$ M), Fc-RB (1  $\mu$ M) and FITC- $\beta$ -CD/Fc-RB (1  $\mu$ M); b) fluorescence emissions of FITC- $\beta$ -CD/Fc-RB (1  $\mu$ M) before (red) and after (green) reaction with H<sub>2</sub>O<sub>2</sub> (150  $\mu$ M) for 30 min; c) fluorescence emission spectra of FITC- $\beta$ -CD and Fc-RB at different molar ratios of 1:0, 1:0.2, 1:0.5, 1:0.7, 1:1 and 0:1; (d) Fold increase of RB/FITC emission ratio (585/515 nm) after 30 min incubation of FITC- $\beta$ -CD/Fc-RB (1  $\mu$ M) with desired concentrations of H<sub>2</sub>O<sub>2</sub>. Error bars represent  $\pm$  standard deviation. \* $p < 0.05$ .

offer sufficient dynamic range to distinguish different H<sub>2</sub>O<sub>2</sub> levels in cancer cells and normal cells. In order to verify the relationship between the fluorescence and the host/guest ratio, the fluorescence emission spectra with different ratios of FITC- $\beta$ -CD to Fc-RB were also detected. Figure 4c shows that the emission from the acceptor (RB, ~585 nm) enhances with the increase of Fc-RB.

In order to investigate its detection limit, FITC- $\beta$ -CD/Fc-RB nanoparticles (1  $\mu$ M) were incubated with indicated concentration of H<sub>2</sub>O<sub>2</sub> (0–150  $\mu$ M). Then the fluorescence emissions at 515 vs 585 nm ( $\lambda_{\text{ex}}=450$  nm) were measured. Figure S9 (see the Supporting Information) shows that the fluorescence lifetime of FITC- $\beta$ -CD/Fc-RB is 2.46 ns. In this study, the FRET ratio change ( $R/R_0$ ) is determined by dividing the ratio of 515/585 nm emissions at each concentration ( $R$ ) by the ratio before H<sub>2</sub>O<sub>2</sub> addition ( $R_0$ ). In the physiologically relevant range, this assay can establish an approximately linear dependence of FITC- $\beta$ -CD/Fc-RB nanoparticles' FRET ratio change on H<sub>2</sub>O<sub>2</sub> concentration, and the detection limit of the FITC- $\beta$ -CD/Fc-RB nanoparticles is about 10  $\mu$ M (Figure 4d and Figure S10 in the Supporting Information).

## Detection of hydrogen peroxide in living cells

Biocompatibility is an important consideration factor for materials working as sensors. Therefore, cytotoxicity of FITC- $\beta$ -CD, Fc-RB and FITC- $\beta$ -CD/Fc-RB nanoparticles in HeLa cells (a human uterine cervix carcinoma cell line) was evaluated by methyl tetrazolium (MTT) assay. Figure 5 indicates that after 24 h incubation in HeLa cells, the cell viability is still over 84% when the final concentration of FITC- $\beta$ -CD/Fc-RB nanoparticles' aqueous solution reaches up to 5  $\mu$ M, which helps to decide what concentration should be used to detect the H<sub>2</sub>O<sub>2</sub> in living cells. It also shows that complexation of FITC- $\beta$ -CD and Fc-RB reduces the cytotoxicity of the Fc-RB guest.<sup>[16]</sup>

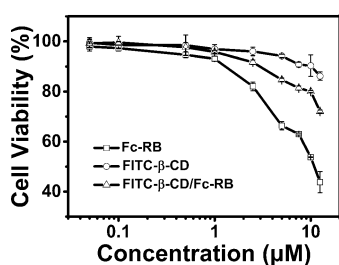


Figure 5. Cytotoxicity of FITC- $\beta$ -CD, Fc-RB and FITC- $\beta$ -CD/Fc-RB nanoparticles in HeLa cells.

The cellular uptake of FITC- $\beta$ -CD/Fc-RB nanoparticles was investigated by flow cytometric measurements. As depicted in the flow cytometry curves in Figures S11–S13 in the Supporting Information, the relative fluorescence intensity of HeLa cells and L929 cells (a mouse fibroblasts cell line, normal cells) pretreated by the FITC- $\beta$ -CD/Fc-RB nanoparticles with or without H<sub>2</sub>O<sub>2</sub> is increasing as the incubation time rises from 5 to 60 min. Figure 6 shows that the fluorescence intensity of cells increases with the increase of incubation time, attributing to the cellular uptake of more and more FITC- $\beta$ -CD/Fc-RB nanoparticles by HeLa and L929 cells. The FRET ratio change is also determined by dividing the fluorescence intensity of RB ( $R$ ) by the fluorescence intensity of FITC ( $R_0$ ). Considering H<sub>2</sub>O<sub>2</sub> levels in cancer cells are higher than those in normal cells, we incubated normal cells with H<sub>2</sub>O<sub>2</sub> (50  $\mu$ M) of cancer cell level as control to judge if the H<sub>2</sub>O<sub>2</sub> in HeLa cells works and disrupts the FRET effect of FITC- $\beta$ -CD/Fc-RB nanoparticles in this experiment. As can be seen in Figure 6, the fold change of HeLa and L929 incubated with H<sub>2</sub>O<sub>2</sub> (50  $\mu$ M) firstly declines and then reaches a plateau, while the fold change of L929 without H<sub>2</sub>O<sub>2</sub> firstly increases and then reaches a plateau, which comes as a result of the FRET effect “on” in L929 cells. Because of the FRET effect, the fluorescence of RB is increasing faster than the fluorescence of FITC.

The fluorescence spectroscopic studies show that the self-assembled FITC- $\beta$ -CD/Fc-RB nanoparticles in aqueous solution can emit strong red and green fluorescence before and after addition of H<sub>2</sub>O<sub>2</sub>, respectively, which indicates that the FITC- $\beta$ -CD/Fc-RB nanoparticles has potential in cell imaging. The fluorescence microscopic measurements were conducted to assess

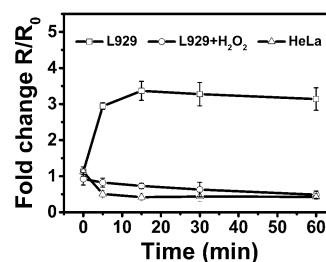


Figure 6. Fold change in RB/FITC emission ratio detected by flow cytometry.

the imaging efficiency of FITC- $\beta$ -CD, Fc-RB and FITC- $\beta$ -CD/Fc-RB nanoparticles (5  $\mu$ M) in HeLa and L929 cells with or without H<sub>2</sub>O<sub>2</sub> (50  $\mu$ M) (Figures S14–S16 in the Supporting Information). When incubated with free FITC- $\beta$ -CD or Fc-RB, both HeLa and L929 cells show strong green fluorescence or red fluorescence. However, if incubated with FITC- $\beta$ -CD/Fc-RB nanoparticles, HeLa cells and L929 cells with 50  $\mu$ M H<sub>2</sub>O<sub>2</sub> show bright green fluorescence while L929 cells show little green fluorescence, because of the disruption of the FRET effect by H<sub>2</sub>O<sub>2</sub>.

The cellular uptake and FRET effect of FITC- $\beta$ -CD/Fc-RB nanoparticles were further studied by confocal laser scanning microscopy (CLSM). For the measurement, HeLa and L929 cells were cultured with FITC- $\beta$ -CD/Fc-RB nanoparticles for 1 h before observation. HOECHST 33342 was used to stain the nuclei and the pretreated cells were observed by Nikon A1Si. Figure 7 shows that the green and red fluorescence of FITC- $\beta$ -CD/Fc-RB mainly appears in the cytoplasm, suggesting that the FITC- $\beta$ -CD/Fc-RB nanoparticles are efficiently internalized by HeLa and L929 cells, and mainly reside in cytoplasm. The green fluorescence of FITC- $\beta$ -CD/Fc-RB nanoparticles could barely be seen in the L929 cells while it could be clearly seen in the HeLa cells, implying that in the presence of H<sub>2</sub>O<sub>2</sub>, cleavage of FITC- $\beta$ -CD/Fc-RB amphiphile and subsequent collapse of supramolecular nanoparticles lead to disruption of the FRET. Thus, the FRET effect is “on” in the L929 cells and “off” in the HeLa cells. In order to judge whether it is the H<sub>2</sub>O<sub>2</sub> in HeLa cells that works and disrupts the FRET effect of FITC- $\beta$ -CD/Fc-RB nanoparticles, L929 cells incubated with 50  $\mu$ M H<sub>2</sub>O<sub>2</sub> were used as control. As can be seen in Figure 7b, the performance is almost the same as fluorescence in HeLa cells. The red fluorescence in HeLa cells and L929 cells incubated with H<sub>2</sub>O<sub>2</sub> of 50  $\mu$ M is obviously lighter than red fluorescence in L929, which confirms the change of FRET from “off” to “on”.

## Conclusion

In summary, we have developed a supramolecular system of fluorescent nanoparticles self-assembled from FITC- $\beta$ -CD/Fc-RB amphiphile with appropriate in vitro FRET effect for H<sub>2</sub>O<sub>2</sub> detection in cancer cells. The DLS and TEM data clearly show that the FITC- $\beta$ -CD/Fc-RB amphiphile based on host-guest interaction can self-assemble into nanoparticles in water and be stable under physiological conditions with the help of hydrophilic/hydrophobic interaction. Moreover, in the fluorescent experiments, the nanoparticles are highly sensitive to H<sub>2</sub>O<sub>2</sub> and its low micromolar sensitivity ( $\sim$ 10  $\mu$ M) makes it effective to

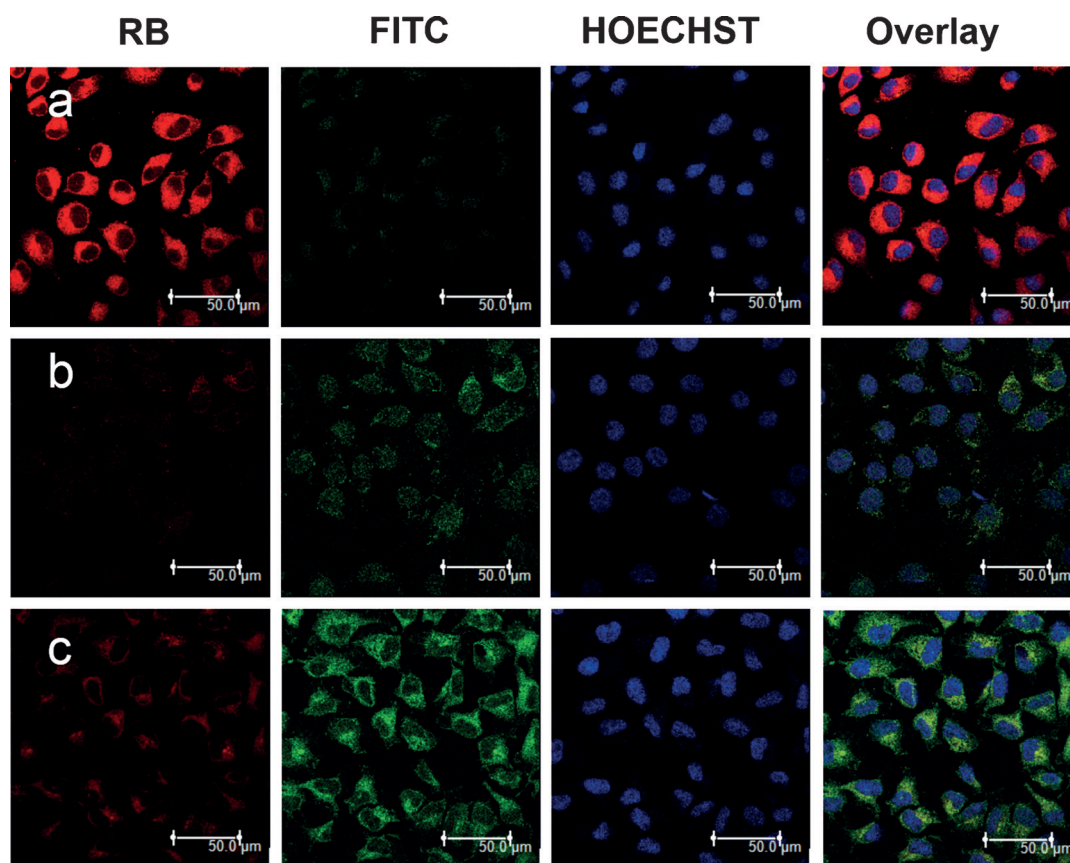


**Figure 7.** Confocal fluorescence images of HeLa and L929 cells.<sup>[11]</sup> Images displayed show emission intensities collected in optical windows between 500 and 600 nm with an excitation wavelength of 488 nm for FITC- $\beta$ -CD/Fc-RB. a) L929 cells incubated with 5  $\mu$ M FITC- $\beta$ -CD/Fc-RB; b) L929 cells incubated for 4 h with 50  $\mu$ M H<sub>2</sub>O<sub>2</sub> and 5  $\mu$ M FITC- $\beta$ -CD/Fc-RB; c) HeLa cells incubated with 5  $\mu$ M FITC- $\beta$ -CD/Fc-RB for 60 min at 37 °C; scale bars 50.0  $\mu$ m.

react with endogenous levels of H<sub>2</sub>O<sub>2</sub> in cancer cells. The in vitro studies verify that after being internalized by cancer cells and then disrupted by endogenous H<sub>2</sub>O<sub>2</sub>, FITC- $\beta$ -CD/Fc-RB nanoparticles can detect H<sub>2</sub>O<sub>2</sub> in cancer cells by the change of FRET from “on” to “off”. Based on these promising results, we anticipate that this supramolecular mechanism from the combination of host-guest interaction and hydrophilic/hydrophobic interaction should be useful in creating novel multi-functional sensors for imaging and detection in living systems.

## Experimental Section

**Materials and instrumentation:**  $\beta$ -Cyclodextrin purchased from Clodextrin Chem Sinopharm Chemical Reagent Co. Ltd. was dried for 48 h at 60 °C in a vacuum oven before use. Other chemicals were got from commercial suppliers such as Alfa, Sigma-Aldrich, TCI and used without further purification. All solvents were purified prior to use. Varian Mercury plus 400 NMR spectrometer (400 MHz) was used to record <sup>1</sup>H NMR spectra with deuterium oxide (D<sub>2</sub>O) or dimethyl sulfoxide-*d*<sub>6</sub> ([D<sub>6</sub>]DMSO) as solvents at 20 °C. And the chemical shifts were referenced to deuterated solvents' peaks: D<sub>2</sub>O (4.80 ppm), [D<sub>6</sub>]DMSO (2.48 ppm). Thermo Electron-EV300 UV/Vis spectrophotometer was used to measure UV/Vis absorption of the materials at 25 °C. PTI-QM/TM/IM steady-state & time-resolved fluorescence spectrofluorometer was used to record the fluorescence emission spectra. And the optimal excitation wavelength of the

sample solutions was set at 450 nm based on the maximum intensity in the excitation spectra.

**Synthesis and characterization:** Compound 1: Tetraglycol (1.73 mL, 10 mmol), DCC (247.6 mg, 1.2 mmol) and DMAP (24.4 mg, 0.2 mmol) were dissolved in CH<sub>2</sub>Cl<sub>2</sub> (20 mL) and to which 1 mmol Rhodamine B in CH<sub>2</sub>Cl<sub>2</sub> was added slowly in 0 °C. Then the mixture was heated to 25 °C and reacted overnight with stirring. After evaporating, the crude product was purified by silica gel column chromatography using CH<sub>2</sub>Cl<sub>2</sub>/CH<sub>3</sub>OH mixture. Yield: 357 mg, 53%. <sup>1</sup>H NMR (400 MHz, [D<sub>6</sub>]DMSO, 20 °C):  $\delta$  = 8.27 (dd,  $J$  = 7.8, 1.2 Hz, 1H), 7.92 (td,  $J$  = 7.5, 1.4 Hz, 1H), 7.86 (td,  $J$  = 7.7, 1.3 Hz, 2H), 7.55–7.49 (m, 1H), 7.09 (dd,  $J$  = 9.5, 2.4 Hz, 2H), 7.06–6.97 (m, 2H), 4.58 (q,  $J$  = 5.6 Hz, 2H), 3.65 (q,  $J$  = 7 Hz, 4H), 3.50–3.43 (m, 10H), 3.06 (s, 8H), 1.21 ppm (t,  $J$  = 7.0 Hz, 12H).

Compound 2: Ferrocenecarboxylic acid (230 mg, 1 mmol), DCC (158.2 mg, 0.77 mmol) and DMAP (171 mg, 1.4 mmol) were dissolved in CH<sub>2</sub>Cl<sub>2</sub> (20 mL) and to which 0.7 mmol compound 1 in CH<sub>2</sub>Cl<sub>2</sub> was added slowly in 0 °C. Then the mixture was heated to at 25 °C and reacted for overnight with stirring. After evaporating, the crude product was purified by silica gel column chromatography using CH<sub>2</sub>Cl<sub>2</sub>/CH<sub>3</sub>OH mixture. Yield: 389 mg, 67%. <sup>1</sup>H NMR (400 MHz, [D<sub>6</sub>]DMSO, 20 °C):  $\delta$  = 8.26 (dd,  $J$  = 7.8, 1.1 Hz, 1H), 7.92 (td,  $J$  = 7.5, 1.4 Hz, 1H), 7.85 (td,  $J$  = 7.7, 1.3 Hz, 2H), 7.53–7.48 (m, 1H), 7.07 (dd,  $J$  = 9.6, 2.3 Hz, 2H), 7.00 (s, 2H), 6.99–6.95 (m, 1H), 4.78–4.68 (m, 2H), 4.51–4.41 (m, 2H), 4.22 (s, 4H), 3.65 (dt,  $J$  = 14.6, 6.0 Hz, 8H), 3.01 (s, 4H), 1.21 ppm (dd,  $J$  = 13.4, 6.5 Hz, 12H).

**Compound 3:** According to the literature procedure,<sup>[13]</sup> dry  $\beta$ -cyclodextrin (25.0 g, 22.0 mmol) was dissolved in 0.4 M aqueous NaOH (250 mL) and cooled down to 0 °C, followed by the addition of *p*-toluenesulfonyl chloride (17.5.0 g, 92 mmol) in small portions under vigorous stirring over 10 min into the solution. Then the resulting suspension was stirred for 30 min below 5 °C, and filtered quickly. Hydrochloric acid was used to neutralize the filtrate to pH 8.5 and stirred for another 1 h. The resultant precipitate was filtered off, rinsed several times with water and dried at 60 °C for 48 h. Yield: 8.58 g, 6.85 mmol, 30%. <sup>1</sup>H NMR (400 MHz, [D<sub>6</sub>]DMSO, 20 °C):  $\delta$  = 7.73 (d, *J* = 8.3 Hz, 2H), 7.41 (d, *J* = 8.2 Hz, 2H), 5.70 (s, 12H), 4.80 (dd, *J* = 15.3, 11.7 Hz, 7H), 4.58–4.05 (m, 7H), 3.81–3.41 (m, 28H), 3.27 (dq, *J* = 18.8, 9.3 Hz, 14H), 2.40 ppm (d, *J* = 6.9 Hz, 3H).

**Compound 4:**<sup>[13]</sup> Compound 3 (5.0 g) was reacted with excess amount of EDA (30 mL) at 75 °C for 4 h. Then the mixture was cooled to room temperature and cold acetone (30 mL) was added. The precipitate was repeatedly dissolved in water (30 mL) and then poured into cold acetone (50 mL) three times to remove the unreacted EDA. The sample obtained was dried at 50 °C for 3 d in a vacuum oven, and  $\beta$ -CD-EDA was obtained (2.3 g, 49%). <sup>1</sup>H NMR (400 MHz, D<sub>2</sub>O, 20 °C):  $\delta$  = 4.91 (d, *J* = 19.0 Hz, 7H), 3.77 (ddd, *J* = 27.5, 16.4, 6.8 Hz, 28H), 3.57–3.39 (m, 14H), 2.92 (d, *J* = 11.0 Hz, 1H), 2.70 (s, 3H), 2.59 ppm (d, *J* = 6.1 Hz, 2H).

**Compound 5:** Compound 4 (213 mg, 0.2 mmol) was dissolved in 15 mL DMF, to which 0.22 mmol FITC in DMF was added slowly at 0 °C. Then the mixture was heated to at 25 °C and reacted for another 4 h with vigorous stirring. The reaction solution was evaporated to 1 mL and precipitated in acetone (15 mL), and the precipitate was filtered. After repeating the operation above for three times, the collected sample was purified by silica gel column chromatography using *n*-propyl alcohol/H<sub>2</sub>O/ammonia water mixture and dried in vacuum oven at 60 °C for 3 d. <sup>1</sup>H NMR (400 MHz, [D<sub>6</sub>]DMSO, 20 °C):  $\delta$  = 8.4 (s, 1H), 7.79 (s, 1H), 7.14 (d, *J* = 8.6 Hz, 1H), 6.67 (s, 2H), 6.57 (q, *J* = 8.7 Hz, 4H), 5.71 (s, 7H), 4.80 (s, 7H), 3.62 (s, 37H), 2.87 ppm (s, 1H).

**Self-assembly of FITC- $\beta$ -CD/Fc-RB in mixed solvents:** Compound 2 (3.32 mg, 0.004 mmol) and compound 5 (6.26 mg, 0.004 mmol) were dissolved in DMF (1 mL), respectively, mixed together and stirred for 6 h. Later the mixture was added dropwise into 8 mL of ultrapure water with stirring, followed by dialysis in a 1000 Da dialysis bag against deionized water to remove DMF. After 24 h, the solution was diluted to 20 mL by adding water to obtain an aggregate solution with a concentration of 200  $\mu$ M for further experiments.

All of the above reactions were done in the dark, and all compounds were characterized by <sup>1</sup>H and <sup>13</sup>C nuclear magnetic resonance.

**Cell experiments:**<sup>[17]</sup> All cells were cultured at 37 °C, 5% CO<sub>2</sub> in a humid incubator. And the HeLa cancer cells and L929 normal cells were incubated in DMEM (Dulbecco's Modified Eagle's Medium) with 10% FBS (Fetal Bovine Serum), and 1% antibiotics. And the confluent cells were sub-cultured every 3 days following standard procedure.

The MTT method<sup>[17]</sup> was performed in HeLa cells to evaluate the cytotoxicity of FITC- $\beta$ -CD/Fc-RB. Cells were seeded into 96-well plates with a density of 5  $\times$  10<sup>3</sup> cells/well in 200  $\mu$ L medium and cultured until 70–80% confluence. After incubation for another day, the culture medium was carefully removed and 200  $\mu$ L of medium with 50  $\mu$ L serial concentrations of FITC- $\beta$ -CD/Fc-RB nanoparticles was added. After grown for another day, 20  $\mu$ L MTT assay stock solution with a concentration of 5 mg mL<sup>-1</sup> in PBS was

added to each well. And after 4 h incubation, the supernatant was removed, followed by the addition of 200  $\mu$ L DMSO to dissolve the obtained blue formazan crystals. PerkinElmer 1420 Multi-label counter was used to measure the absorbance with an excitation wavelength of 490 nm.

The flow cytometry analysis<sup>[17]</sup> was also conducted to assess the cell internalization of FITC- $\beta$ -CD/Fc-RB and the ability to detect the H<sub>2</sub>O<sub>2</sub> in HeLa and L929 cells correspondently. Because of their own fluorescence, the supramolecular fluorescent nanoparticles were added to the cells directly and incubated for indicated time that is 5, 15, 30 and 60 min. The cellular uptake experiments were performed on flow cytometry. Firstly, cells were seeded in six-well incubated for another day. Then FITC- $\beta$ -CD/Fc-RB were dissolved in DMEM culture medium with a final concentration of 5  $\mu$ M and added to each well. After that the cells were cultured at 37 °C for 5, 15, 30 and 60 min. Finally, the cells were collected by removing the supernatant, washing with cold PBS buffer several times, and treating with Trypsin. 1.0  $\times$  10<sup>4</sup> cells were counted and analysis was conducted with BD FACSCalibur flow cytometer and CELLQuest software.

Moreover, the confocal laser scanning microscopy (CLSM) measurements<sup>[17]</sup> were performed to evaluate the imaging efficiency and FRET effect of FITC- $\beta$ -CD/Fc-RB nanoparticles in HeLa cells and L929 cells. Cells were seeded in six-well plates with a density of 2  $\times$  10<sup>5</sup> cells per well in 2 mL of complete DMEM. After incubation for another day, culture medium was removed and 2 mL DMEM medium containing 5  $\mu$ M of FITC- $\beta$ -CD/Fc-RB nanoparticles was added. The cells were cultured at 37 °C for desired time, followed by being rinsed with cold PBS buffer, fixed with 4% paraformaldehyde for 30 min at 25 °C. Then the slides were washed with cold PBS buffer for several times and HOECHST 33342 was used to stain the nuclei for 15 min. After being washed with cold PBS buffer, the slides were mounted and observed with a fluorescence microscope (Leica DMI6000 B) and a confocal laser scanning microscope (Nikon A1Si). What's more, in order to make sure if the hydrogen peroxide in the HeLa cells worked, L929 cells incubated with H<sub>2</sub>O<sub>2</sub> of 50  $\mu$ M were also used in this experiment as control.

**NMR spectroscopy:** Varian Mercury Plus 400 MHz spectrometer was used to record NMR spectra with [D<sub>6</sub>]DMSO, and D<sub>2</sub>O as solvents at 20 °C.

**FTIR spectroscopy:** Paragon 1000 instrument was used to record the FTIR spectra through the KBr sample holder method.

**Transmission electron microscopy (TEM):** JEOL JEM-100CX-II instrument was used to investigate the morphology of the nanoparticles at a voltage of 200 kV. The nanoparticle solution was dropped onto the carbon-coated copper grids and then air-dried before measurement.

**Dynamic light scattering (DLS):** Malvern Zetasizer Nano S apparatus (Malvern Instruments Ltd) equipped with a 4.0 mW He/Ne laser operating at  $\lambda$  = 633 nm was used to do the DLS measurements.

**UV/Vis spectrophotometry:** Thermo Evolution 300 UV/Vis spectrophotometer was used to record the UV/Vis spectra in the range of 200–650 nm.

**MTT:** PerkinElmer 1420 Multi-label counter was used to record the absorbance with an excitation wavelength of 490 nm.

## Acknowledgements

This work was financially supported by the National Basic Research Program (2015CB931801), National Natural Science

Foundation of China (51473093), and Science Foundation Ireland (SFI), SFI Principal Investigator Programme.

**Keywords:** fluorescence · FRET · hydrogen peroxide · nanoparticles · supramolecular assembly

- [1] a) E. A. Veal, A. M. Day, B. A. Morgan, *Mol. Cell* **2007**, *26*, 1–14; b) S. G. Rhee, *Science* **2006**, *312*, 1882–1883; c) J. R. Stone, S. Yang, *Antioxid. Redox Signaling* **2006**, *8*, 243–270; d) B. D'Autréaux, M. B. Toledano, *Nat. Rev. Mol. Cell Biol.* **2007**, *8*, 813–824; e) M. Giorgio, M. Trinei, E. Migliaccio, P. G. Pelicci, *Nat. Rev. Mol. Cell Biol.* **2007**, *8*, 722–728; f) B. C. Dickinson, C. J. Chang, *J. Am. Chem. Soc.* **2008**, *130*, 9638–9639; g) L. B. Poole, K. J. Nelson, *Curr. Opin. Chem. Biol.* **2008**, *12*, 18–24.
- [2] T. Finkel, M. Serrano, M. A. Blasco, *Nature* **2007**, *448*, 767–774; b) S. Reuter, S. C. Gupta, M. M. Chaturvedi, B. B. Aggarwal, *Free Radical Biol. Med.* **2010**, *49*, 1603–1616.
- [3] N. Houstis, E. D. Rosen, E. S. Lander, *Nature* **2006**, *440*, 944–948.
- [4] a) R. M. Touyz, E. L. Schiffrin, *Histochem. Cell Biol.* **2004**, *122*, 339–352; b) H. Cai, *Cardiovasc. Res.* **2005**, *68*, 26–36.
- [5] a) K. J. Barnham, C. L. Masters, A. I. Bush, *Nat. Rev. Drug Discovery* **2004**, *3*, 205–214; b) M. T. Lin, M. F. Beal, *Nature* **2006**, *443*, 787–795.
- [6] a) S. D. Lim, C. Sun, J. D. Lambeth, F. Marshall, M. Amin, L. Chung, J. A. Petros, R. S. Arnold, *Prostate* **2005**, *62*, 200–207; b) S. V. Lennon, S. J. Martin, T. G. Cotter, *Cell Proliferation* **1991**, *24*, 203–214; c) F. Antunes, E. Cadenas, *Free Radical Biol. Med.* **2001**, *30*, 1008–1018.
- [7] D. Lee, S. Khaja, J. C. Velasquez-Castano, M. Dasari, C. Sun, J. Petros, W. R. Taylor, N. Murthy, *Nat. Mater.* **2007**, *6*, 765–769.
- [8] a) E. W. Miller, O. Tulyanthan, E. Y. Isacoff, C. J. Chang, *Nat. Chem. Biol.* **2007**, *3*, 263–267; b) D. Srikun, E. W. Miller, D. W. Dornaille, C. J. Chang, *J. Am. Chem. Soc.* **2008**, *130*, 4596–4597; c) R. Weinstain, E. N. Savariar, C. N. Felsen, C. N. Felsen, R. Y. Tsien, *J. Am. Chem. Soc.* **2014**, *136*, 874–877.
- [9] J. L. Lyon, K. J. Stevenson, *Anal. Chem.* **2006**, *78*, 8518–8525.
- [10] a) R. J. Dong, Y. Su, S. R. Yu, Y. F. Zhou, Y. F. Lu, X. Y. Zhu, *Chem. Commun.* **2013**, *49*, 9845–9847; b) M. Nakahata, Y. Takashima, H. Yamaguchi, A. Harada, *Nat. Commun.* **2011**, *2*, 511–516; c) C. Conrado, C. M. Juan, V. Reynaldo, *Langmuir* **2008**, *24*, 7654–7657; d) R. J. Dong, Y. F. Zhou, X. H. Huang, X. Y. Zhu, *Adv. Mater.* **2015**, *27*, 498–526; e) C. Wang, Y. Guo, Y. Wang, H. Xu, X. Zhang, *Chem. Commun.* **2009**, 5380–5382.
- [11] a) G. Yu, X. Zhou, Z. Zhang, F. Huang, *J. Am. Chem. Soc.* **2012**, *134*, 19489–19497; b) G. Yu, M. Xue, Z. Zhang, F. Huang, *J. Am. Chem. Soc.* **2012**, *134*, 13248–13251; c) G. Yu, K. Jie, F. Huang, *Chem. Rev.* **2015**.
- [12] a) P. K. Pallela, T. Chiku, M. J. Carvan, *Anal. Biochem.* **2006**, *352*, 265–273; b) Y. Nakamura, K. Kogure, S. Futaki, *J. Controlled Release* **2007**, *119*, 360–367; c) H. J. Kong, C. J. Kim, N. Huebsch, *J. Am. Chem. Soc.* **2007**, *129*, 4518–4519; d) F. Olivero, F. Carniato, C. Bisio, *Chem. Asian J.* **2014**, *9*, 158–165.
- [13] a) R. C. Petter, J. S. Salek, C. T. Sikorski, G. Kumaravel, F. T. Lin, *J. Am. Chem. Soc.* **1990**, *112*, 3860–3868; b) D. Vitzitui, C. S. Walkinshaw, B. I. Gorin, G. R. Thatcher, *J. Org. Chem.* **1997**, *62*, 8760–8766; c) B. L. May, S. D. Kean, C. J. Easton, S. F. Lincoln, *J. Chem. Soc. Perkin Trans. 1* **1997**, 3157–3160.
- [14] a) A. Harada, S. Takahashi, *J. Chem. Soc. Chem. Commun.* **1984**, 645–646; b) F. Hapiot, S. Tilloy, E. Monflier, *Chem. Rev.* **2006**, *106*, 767–781; c) W. S. Jeon, K. Moon, S. H. Park, *J. Am. Chem. Soc.* **2005**, *127*, 12984–12989.
- [15] D. Taura, S. Li, A. Hashidzume, *Macromolecules* **2010**, *43*, 1706–1713.
- [16] H. Takuto, H. Fumio, *Bioorg. Med. Chem.* **2009**, *17*, 6015–6019.
- [17] a) S. Yu, R. Dong, J. Chen, D. Yan, *Biomacromolecules* **2014**, *15*, 1828–1836; b) B. Liu, D. Wang, G. Li, X. Zhu, *Polym. Chem.* **2015**, *6*, 3460–3471.

Received: April 2, 2015

Published online on July 1, 2015